Materials and Design 189 (2020) 108546

Contents lists available at ScienceDirect

Materials and Design

journal homepage: www.elsevier.com/locate/matdes

A validated finite element analysis procedure for porous structures

Sergio Ruiz de Galarreta [a,*], Jonathan R.T. Jeffers [b], Shaaz Ghouse [b]

[a] Department of Mechanical Engineering and Materials, Universidad de Navarra, TECNUN Escuela de Ingenieros, Paseo Manuel de Lardizabal, 13, 20018 San Sebastian, Spain
[b] Department of Mechanical Engineering, Imperial College London, London SW7 2AZ, United Kingdom

HIGHLIGHTS

- An accurate finite element analysis procedure is defined to model lattice structures.
- Numerical and experimental results are in good agreement.
- Accurate definition of the actual material is necessary to obtain reliable results.
- Accurate representation of test conditions is necessary to obtain reliable results.

GRAPHICAL ABSTRACT

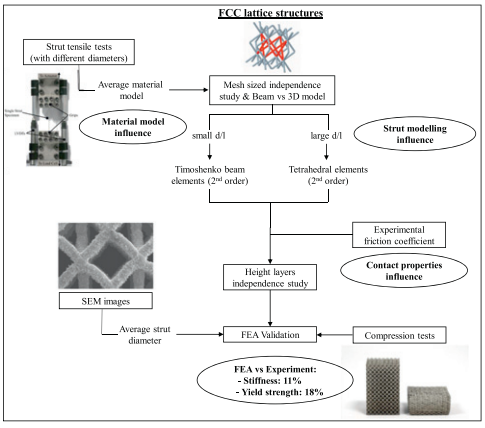

ARTICLE INFO

Article history:
Received 13 November 2019
Received in revised form 31 January 2020
Accepted 3 February 2020
Available online 4 February 2020

Keywords:
Lattice structures
Finite element analysis
Mechanical testing
Additive manufacturing
Struts

ABSTRACT

Cellular materials are gaining interest thanks to developments in additive manufacturing. Whilst Finite Element Analysis (FEA) is commonly used to obtain the mechanical behaviour of these structures, different modelling and simulation methodologies are followed in literature. Consequently, there is not a clear procedure to accurately evaluate the mechanical properties of porous structures. This study presents a method to perform FEA of lattice structures with accurate results. All inputs required to simulate compression testing of lattices in FEA were investigated, these included the modelling type, element size, number of unit cells required, boundary conditions and the material model. The effect of these variables on the modulus and yield strength of a lattice structure was studied.

Lattices with two unit cell structures, varying unit cell sizes and relative densities were additively manufactured in stainless steel, compression tested and compared to FE simulations. The material model for the FE simulations was obtained from tensile testing individual micro-struts of varying diameters. FE simulation results were in good agreement with the experimental results with an average error for the modulus and yield strength of ~10% and 17% respectively. The methodology presented should provide a foundation to accelerate development and adoption of these structures.

* Corresponding author.
E-mail address: sruiz@tecnun.es (S. Ruiz de Galarreta).

https://doi.org/10.1016/j.matdes.2020.108546

1. Introduction

Due to developments in new manufacturing technologies such as additive manufacturing (AM), cellular materials are receiving considerably more attention as they can now be manufactured with a level of control not previously possible. Cellular materials also known as lattice structures are types of porous materials which are typically formed by a periodic or stochastic arrangement of beams/struts forming a three-dimensional framework. They can also be made up of surfaces such as honeycombs or triply periodic structures. AM has increased the design freedom, the porosity control and the accuracy of these structures overcoming some limitations found during conventional manufacturing of these materials [1].

The superior specific stiffness and strength of lattice structures [2] make them ideal to design light-weight structures [3], additionally they possess good energy absorption and heat transfer capabilities and thus have many applications in industries such as aerospace, aeronautic and automotive. Their low mass, potentially low modulus and porous nature also make them suited for bone ingrowth applications for the biomedical industry, particularly in the field of orthopaedic implants [4]. Due to the diverse applications of lattice structures, there is significant interest in their mechanical behaviour and therefore numerous numerical and experimental studies have been carried out. The primary benefit of experimental testing is that the results reflect the actual behaviour of the material and are directly translatable to the real-world application. However, the down-side is often a limited design space and a large time and cost associated with manufacturing samples, removing them from the substrate, post-machining and finally testing. Whereas analytical models have the potential to explore a far greater design space in a potentially much cheaper and shorter period of time. Though some analytical models have been developed for unit cells such as body-centered-cubic (BCC) [5,6], diamond [7], face-centered-cubic (FCC) [8] and rhombic dodecahedron [7,9], the mechanical properties of lattice structures are more commonly estimated by Finite Element Analysis (FEA). However, the FEA methodology used for lattice structures can differ greatly between studies.

Previous studies have analysed the mechanical behaviour of different lattice structures under compression by FEA and have compared it to experimental results, however, different approaches were followed regarding boundary conditions. Some researchers [10–12] directly apply a displacement to the top nodes of the structure while fixing the bottom nodes; whilst others introduce two shells in the FEA, representing the platens of the experimental compression test. In the latter works, some researchers consider a frictionless contact between the platens and the lattice [5,6,13,14] whilst others introduce a penalty factor to account for that friction [15–17] or even a bonded contact where sliding is not permitted [18]. Due to the computational cost, beam elements are desirable compared to 3D elements when modelling strut-based lattice structures, however there are again different methods followed when using beam elements. Some researchers model the struts with beams of constant cross section [7,10,19], while in other studies, to account for the higher material concentration around the strut junctions or nodes, the diameter is increased at the nodes by ~20% [5,6,13] or 40% [20] or as in the case of Luxner et al. [21], the stiffness is increased 1000 times in nodal regions.

The material model is another key parameter that affects FEA results, and again various approaches have been followed. Plasticity is usually included in the material model by a number of methods: by an elastic-perfectly-plastic model (i.e. without accounting for the strain hardening) [22], by considering the strain hardening with a bilinear-elastic-plastic model [18], by directly using the material stress-strain data [13] or by using other models such as the Johnson-Cook model to evaluate damage [12,23]. To determine the material model, some studies use mechanical property data provided by the machine manufacturer or test tensile specimens from the bulk AM material [12–14,17,24,25], whilst other studies manufacture and test individual representative struts [6,16]. The advantage of the latter, is that the material model describes the behaviour of the strut including possible imperfections such as diameter deviations, surface roughness or internal micro-porosity. Some studies also physically model these types of imperfections [11,26] as well as other imperfections such as the fracture behaviour of struts [18] and strut 'waviness' [17]. In studies which have tested individual micro-struts [6,16,27] they have found modulus and strength values below that of the bulk material. However, it has not been shown yet how the material properties change as strut diameter increases or at what point it approaches that of the bulk material.

In most studies, FEA results are compared to experimental values, however the FEA methodology followed differs significantly amongst studies and often a systematic approach to developing the model is not described. It must also be noted that strut-based porous structures are often classified by their deformation mechanics. The structure is said to be 'bend-dominated' if struts bend or buckle during compressive loading; alternatively for certain porous structures it is possible for some struts to carry an axial tensile load during compression and these structures are classified as 'stretch-dominated.' It remains unclear how deformation mechanics and different types of cellular geometries will affect the convergence and accuracy of FE simulations. The main purpose of this work is to determine and provide a procedure to perform FEA of a periodic lattice structure under compression with accurate and reliable results when compared to physical mechanical testing at minimum computational cost. This will initially be done on bend-dominated structures, with the view that it can be applied to stretch-dominated structures, stochastic structures and graded structures. The following steps were performed:

- Determine element size/type and the minimum # of unit cells required for both beam and 3D models to achieve convergence of mechanical properties.
- Compare different approaches (beam vs 3D) to model lattice structures.
- Determine whether the boundary conditions have an effect on the minimum number of unit cells required and their influence on mechanical properties.
- Manufacture and uniaxially test individual struts with different diameters to obtain the material model.
- Perform a sensitivity analysis regarding the material model.
- Manufacture and test lattice structures with different relative densities (different strut diameters & different unit cell sizes)
- Compare the elastic modulus and yield strength under compression of the experimental and FEA results.

2. Materials and methods

2.1. Numerical modelling

As the method used to model compression tests by FEA has a significant influence on the results, prior to simulating the experimental tests, a sensitivity analysis of different methodologies was performed. All quasi-static simulations were performed using ABAQUS 2019/Standard software package (Dassault Systems). Two methods were used to model the lattice structures. For the first, an in-house code developed in MATLAB was used to model the struts with 3-node Timoshenko quadratic beam elements (B32). For the second, the lattice structures were designed in PTC CREO 5.0 (PTC Inc.) and meshed in ABAQUS with 3D quadratic tetrahedral elements (C3D10). A modified Face-Centred-Cubic (FCC) structure (all horizontal beams were removed) was used for the FE model

development and validation (Fig. 1). Prior to simulation, a mesh size sensitivity analysis was carried out on both beam and tetrahedral elements. Following this, a convergence study was performed to determine the minimum number of unit cells required in each direction to obtain consistent elastic modulus and yield strength results. The results of the convergence study are presented in Section 3.1.

The FEA model is seen in Fig. 1, for all simulations two rigid shells models were placed at the top and bottom of the lattice structure, each having a reference point at their centre. The reference point of the lower shell was completely fixed, while the reference point of the upper plate was set to progressively deform the lattice structure until it yields (with strains ranging from 3% to 10% depending on the structure). For the solid FE models, symmetry is considered and only one quarter of the structure is studied, constraining the normal displacement of the symmetric faces (Fig. 1). The contact properties between the shells and the lattice structure were set to "hard" in the normal direction and frictionless in the tangential direction (except in 2.1.2). The bilinear elasto-plastic model shown in Table 2 and described in Section 2.2.5 was implemented in all the analyses (except in 2.1.3). Due to the small deformations self-contact between struts was not considered.

To calculate the elastic modulus and yield strength for each structure, the engineering stress-strain curves were derived from the FEA results. Stress was calculated by dividing the reaction force at the reference point of the top shell by the apparent cross-sectional area of the structure, whilst strain was determined by dividing the displacement of the top shell by the initial length of the structure. A regression analysis was performed in the linear region of the stress-strain curve to obtain the elastic modulus. Due to the lack of a distinct peak stress value, the yield strength was measured at a strain offset of 0.2%.

2.1.1. Lattice structure modelling sensitivity analysis

Due to computational cost, some studies use beam elements to model lattices. In most of these studies an increase of the strut diameter close to the nodes is applied to account for the material concentration and to avoid the lack of contact between struts, whilst in others a constant strut cross section is used. To analyse the sensitivity of the results to these approaches, three cases were studied for the FCC structure: struts with constant cross section and struts with an increased diameter in the node regions of 20% and 40% (Fig. 1). The length of the region where the diameter was increased was set to be equal to the strut radius. FCC structures of varying unit cell sizes and strut diameters were studied (Table 1). Identical structures were also modelled with 3D elements to compare the two modelling approaches. Note that length (l) in Table 1 is the length between two nodes and not the total length of the strut nor the unit cell length (Fig. 1).

2.1.2. Boundary conditions sensitivity analysis

To determine the mechanical properties of lattice structures from experimental compression tests, platens are usually lubricated to reduce the effect of friction on lateral deformation. This tangential friction is modelled in FEA with different values in the literature. To analyse its sensitivity on the results, five scenarios were studied: frictionless, friction coefficients equal to 0.1, 0.2 and 0.3 and bonded contact, i.e. no sliding permitted. These contact properties were applied to structure 10 (Table 1) meshed with solid 3D elements. When implementing friction in FEA simulations of lattice structures, the "barrel"-ing effect is observed due to the shear forces at the contact region. Consequently, this will have an influence on the results depending on the height of the structures and therefore the influence of the number of unit cells was studied again. To avoid a huge amount of 3D elements, the width of the FCC structure was set to 12 mm, i.e. 8 unit cells which is the minimum number recommended by Gibson and Ashby [28,29]. Then the number of unit cells in the height of the structure was investigated again, to ensure the stiffness and yield strength converged at minimal computational cost, for each of the five friction boundary conditions.

2.1.3. Material model sensitivity analysis

The material model has a significant influence on the results in FEA simulations. As discussed in Section 2.2.5, single struts of increasing diameter were tested in tension and stress-strain curves were obtained. Due to little variation between curves of different diameters, an average stress-strain curve of all the struts was produced. From this curve, two bilinear elasto-plastic models were derived (Section 3.3). In the first one (A) the yield strength is the intersection between the slopes of the initial stiffness and plastic hardening modulus. In the second one (B), the yield strength was set at an offset of 0.2% of the stress strain curve. These two models together with the actual stress-strain curve were used to model the material of structure 14 (Table 1) and the results were compared. Additionally, the same structure was modelled with the elasto-plastic model B derived from the stress-strain curves of strut 1 and 4 (Table 2). These struts were chosen because they had the greatest yield strength and stiffness deviation from the average model.

2.1.4. FEA of the experimental structures

After the sensitivity analysis of the different variables and methodologies, FEA was performed on the FCC structures that were manufactured and tested experimentally. Strut diameter was taken from the physically manufactured specimens, as discussed in 2.2.3. The width/length of the designed structure was the same as the fabricated structures, while only 5 unit cells were modelled in the height to reduce the number of elements as discussed later in Section 3.2. The structures were meshed with quadratic tetrahedral

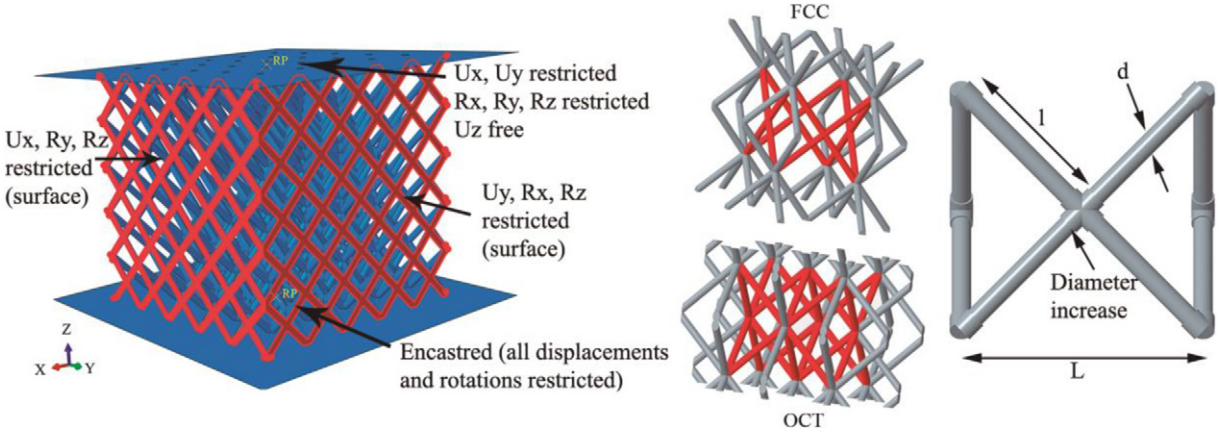

Fig. 1. FEA boundary conditions (left), modified FCC and OCT structures (middle), example of nodal increase and nomenclature (right).

Table 1
FCC Lattice structures for comparing modelling approaches.

Structure	Cell size [mm]	Strut diameter [mm]	d/l ratio [−]	Rel. Density [−]
1	5	0.05	0.014	0.0004
2	5	0.1	0.028	0.0017
3	5	0.2	0.057	0.007
4	1.5	0.1	0.094	0.019
5	5	0.4	0.113	0.026
6	2.5	0.2	0.113	0.026
7	1.5	0.15	0.141	0.041
8	5	0.6	0.170	0.057
9	2.5	0.3	0.170	0.057
10	1.5	0.2	0.189	0.070
11	5	0.8	0.226	0.098
12	2.5	0.4	0.226	0.098
13	1.5	0.25	0.236	0.105
14	1.5	0.3	0.282	0.146
15	2.5	0.5	0.283	0.146
16	1.5	0.35	0.330	0.192

elements. The average bilinear elasto-plastic model B described later in Section 3.3 was used to define the material for all the structures. A penalty factor equal to 0.1 was set in the tangential direction to account for the friction between the structures and the platens. To further investigate the accuracy of the developed FE methodology on other structures; modified octet-truss (OCT) specimens with all horizontal beams removed, were also simulated following the same procedure as above and were compared against experimentally tested specimens.

2.2. Experimental methodology

2.2.1. Specimen design and build file generation

Modified FCC porous specimens were designed in MATLAB (MathWorks Inc.). The structure was defined in a 7 column CSV (comma separated values) format, where each row reflects a single strut. The first 3 columns are the starting x, y & z co-ordinates of the strut, the following 3 columns are the end x, y & z co-ordinates of the strut and the final column is the diameter of the strut. Cuboid specimens were designed with one of two different unit cell sizes: either a 1.5 mm or 2.5 mm unit cell size. The test specimen size was $15 \times 15 \times 22.5$ mm ($10 \times 10 \times 15$ unit cells) and $20 \times 20 \times 30$ mm ($8 \times 8 \times 12$ unit cells) for the 1.5 mm and 2.5 mm unit cell size variants respectively. Ensuring there was a minimum of at least 8 unit cells in the length/width as per the recommendations of Gibson & Ashby [28,29] and a height of at least 1.5× the length/width (as per ISO 13314:2011). Modified OCT porous specimens, to further test the accuracy of the developed FE methodology, were also designed with a 1.5 mm unit size cell and specimen size of $15 \times 15 \times 22.5$ mm ($10 \times 10 \times 15$ unit cells). To understand the material properties of the struts in the FCC and OCT specimens, 80 mm long single struts were designed at the same angle as are present in these structures (45° to the build plate) to be used for tensile testing.

An in-house developed piece of software was used to create slice data and thus generate build files (Fig. 2). For every strut, the software calculates the intersections between the strut and the slice layers. At each intersection a circle or ellipse is generated (based on the angle of the strut) at the specified size. Following Boolean union-ing of these contours on a layer-by-layer basis, the resulting geometries are placed into the file format required by the additive manufacturing system. Traditionally, the area enclosed by these contours are filled in with 'hatch' scans, however in this

Table 2
Elastic modulus, yield and ultimate strength of the uniaxially tested struts.

Strut	SEM diameter (s.d.) [μm]	Average elastic modulus (s.d.) [GPa]	Average yield Strength (s.d.) [MPa]	Average ultimate strength (s.d.) [MPa]
1	176.9 (9.0)	86.3 (2.2)	277.8 (8.1)	642.1 (9.9)
2	205.8 (10.1)	88.8 (14.1)	265.3 (11.9)	570.6 (13.6)
3	247.8 (13.9)	81.7 (3.1)	252.7 (5.9)	567.0 (10.1)
4	289.2 (15.5)	70.6 (2.3)	258.5 (13.0)	529.5 (14.8)
5	325.5 (12.9)	80.4 (2.6)	257.4 (3.3)	562.7 (41.5)
6	362.1 (11.9)	84.2 (4.5)	267.7 (3.7)	560.6 (30.3)
7	408.7 (18.8)	83.9 (0.2)	266.1 (3.6)	563.6 (13.6)
Strut Average		81.3	263.3	575.3

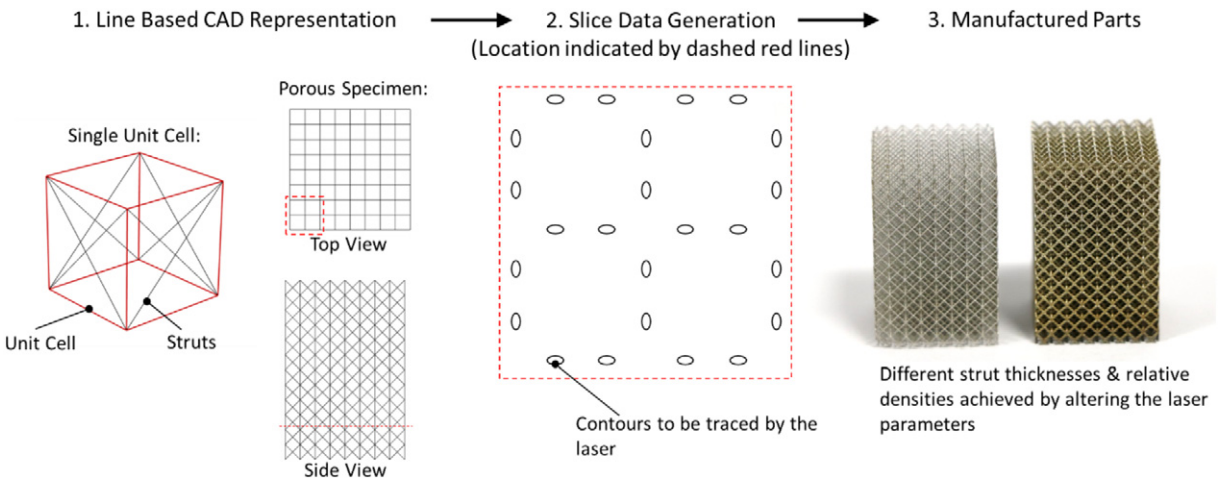

Fig. 2. Manufacturing workflow from specimen design to build file generation to manufacture for the FCC structure.

research, the diameter of the contour scan was set equal to the spot size of the laser (70 μm), this was to ensure it was possible to build small micro-struts and that there was no need for interpolative calculations to generate additional border or hatch scans, strut thickness was then controlled purely by the laser parameters. This method has been described and utilised previously in [30,31]. Laser parameters were assigned on a part-by-part basis. Previous work has established a relationship between strut diameter and laser parameter utilising the above method [31] and consequently for each unit cell size, specimens were built with 5 different strut diameters/laser parameters. Strut diameters were nominally in the range of 170–450 μm to produce relative densities of ~2–20%, as described in Table 4. Single struts for tensile testing were built with all of the laser parameters used for the FCC and OCT structures.

2.2.2. Materials and manufacturing

A Renishaw AM250 metal powder bed fusion system was used to manufacture all specimens. The workings of the AM250 and the manufacturing process has been described in detail previously [30,31]. Specimens were manufactured from Stainless Steel 316 L powder (Carpenter Additive Ltd.) having a spherical shape with a particle size range of 10–45 μm (D_{50}: 27 μm) and built onto mild steel substrates. The lattice structures were removed by electro discharge machining, ground parallel and cleaned ultrasonically in ethanol whilst the single struts were removed by pliers.

2.2.3. Morphological analysis

Overall structure relative density per unique specimen was measured by dry weighing in atmospheric conditions with $n = 5$ (i.e. repeated on 5 identical samples). Relative density was calculated by dividing actual weight by the theoretical weight of the macro volume using a density of 8.1 g/cm^3. Overall dimensions of the structure were taken by a Vernier calliper. Each structure as well as the struts manufactured for tensile testing were imaged using a scanning electron microscope (Hitachi S-3400 N) and consequently strut thickness was measured utilising ImageJ in 20 locations and averaged.

2.2.4. Quasi static compression testing

Quasi-Static compression testing was performed on the lattices to ISO 13314:2011 using a material testing machine (Instron 8872) equipped with a 5 kN load-cell. Specimens were compressed at a constant rate of 2 mm/min. For a given unit cell size and strut diameter, a preliminary sample was compressed to 50% strain to estimate the plateau strength. The estimated plateau strength was the mean of the stresses between 20% and 30% strain (Fig. 3). To determine the elastic modulus and yield strength for a given unit cell size and strut diameter, samples ($n = 5$) were loaded to 50% strain with a hysteresis loop between 70% and 20% of the estimated plateau strength (Fig. 3) to account for the localized plasticity in porous materials which reduces the slope of the initial loading curve [28]. Displacement between the platens was measured at 30 Hz by two LVDTs (RDP D6/05000A) to reduce test-machine compliance errors. Strain was the average LVDT displacement divided by the specimen's initial height and stress (σ) was the measured load divided by the specimen's initial cross-sectional area (calculated from the initial length & width of the specimen). Stress-Strain curves were produced for each test; elastic modulus (E) was the linear regression of the hysteresis loop whilst the yield strength (σ_y) is determined as compressive stress at a plastic compressive strain of 1.0% relative to the elastic modulus (Fig. 3).

2.2.5. Single strut tensile testing

Tensile testing was performed using a materials testing machine (Instron 5570). The gauge length of the strut was 40 mm and was gripped over a 15 mm length either side (Fig. 4). The grips were additively manufactured and struts were sandwiched between one grip featuring a 90° 'v-groove' and one flat grip. Grips with different depths of v-grooves were made to hold the struts of different diameters. Seven different strut diameters (ranging from 170 to 410 μm) were tested and for each diameter two specimens were tested. Displacement between the grips was measured at 30 Hz by two LVDTs (RDP D6/05000A) to get a more accurate measure of strain by reducing test-machine compliance errors (Fig. 4). The small diameter of the struts makes using a clip-on extensometer prohibitively difficult; the LVDTs were validated against a camera system with the benefit of being far faster in terms of data post-processing. Strain was the average LVDT displacement divided by the specimen's initial gauge length and stress (σ) was the measured load divided by the specimen's initial cross-sectional area (calculated from the strut diameter measured from SEM images). Stress-Strain curves were produced for each test; elastic modulus (E) was the linear regression of the initial loading curve whilst the yield strength (σ_y) is determined as compressive stress at a plastic compressive strain of 0.2% relative to the elastic modulus (Fig. 4).

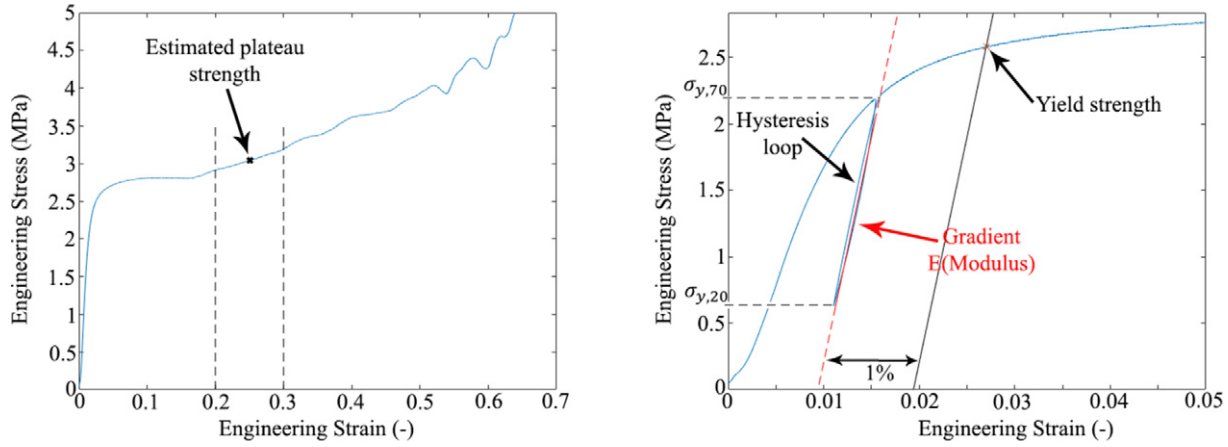

Fig. 3. Preliminary compression test (left) and compression stress-strain curve with hysteresis loop (right).

3. Results

3.1. Lattice structure modelling

For the FCC structure, six quadratic beam elements were found to be appropriate to model each strut, while for the solid mesh, element size ranging from 80 μm to 120 μm (depending on the strut diameter) resulted in the convergence of stiffness and yield strength. When modelling with beam elements, a structure of 14x14x14 unit cells saw convergence of the elastic modulus and yield strength (the difference with a structure of 16x16x16 was <1%). In contrast, for the 3D mesh, structures of 6x6x3 were found to be sufficient, especially when considering the computational cost (the difference with the 8x8x4 structure was <2.5%). It should be mentioned that increasing the height varies the results <1% and therefore the height was set to 3 unit cells to minimize the number of elements used. Also, if structures with large height-length ratios were analysed, buckling effects would appear due to the slenderness of the structures affecting the mechanical properties. Element size and number of unit cells sensitivity analyses for the beam and solid mesh are illustrated in Fig. 5.

The elastic modulus and yield strength of the FCC structures displayed in Table 1 are illustrated in Fig. 6. When modelling the structure with beam elements, increasing the diameter in the nodal regions, results in an increase of both the elastic modulus and yield strength. When increasing the diameter 20% in the nodal regions, the elastic modulus and yield strength increases by 12.85% (3.27%) and 11.64% (3.18%) respectively, and 19.01% (4.90%) and 12.29% (3.51%) when increasing the diameter up to 40%.

Fig. 7 shows the errors between the beam model with constant cross section and the 3D model. As it can be observed for small d/l ratios (or small relative densities) the errors in elastic modulus converge to 14% and therefore for d/l values below 0.06, the beam model approximation is acceptable. However, for larger d/l ratios the errors increase almost linearly making the difference between the beam model and 3D elements significant. A similar trend is observed with the beam models with a 20% and 40% diameter increase in the node regions, with errors converging to 6% and 2% respectively at small d/l ratios and increasing as the d/l ratio goes up. It is also seen that the error depends solely on the d/l ratio (i.e. relative density) rather than the unit cell size.

3.2. Boundary conditions

Fig. 8 shows the convergence of the elastic modulus of the FCC structure for five different boundary conditions with varying number of unit cells in height. For a frictionless contact, modelling 3

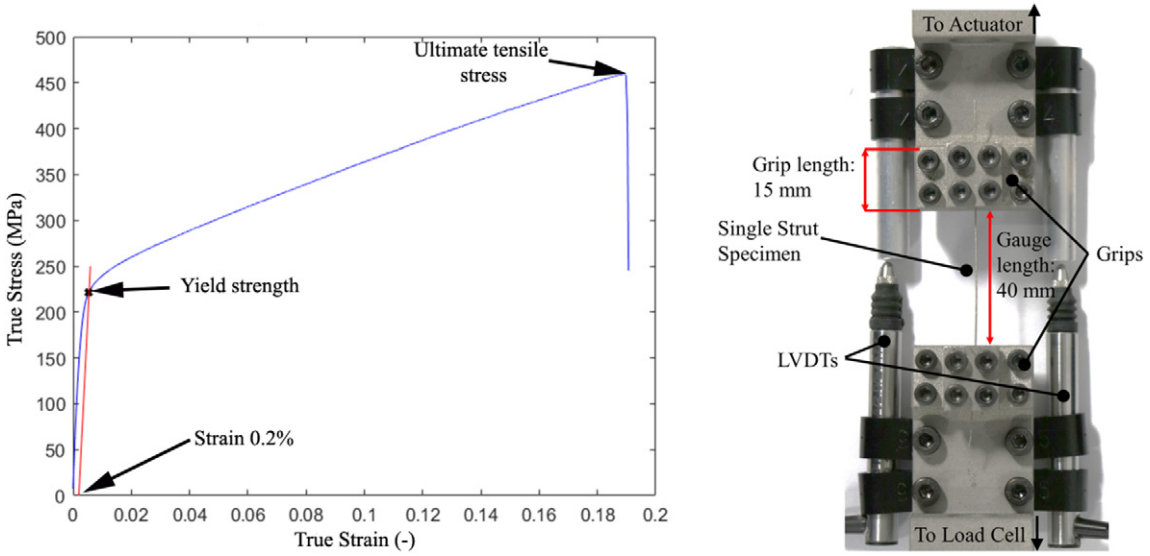

Fig. 4. Strut stress strain curve (left) and tensile test setup (right).

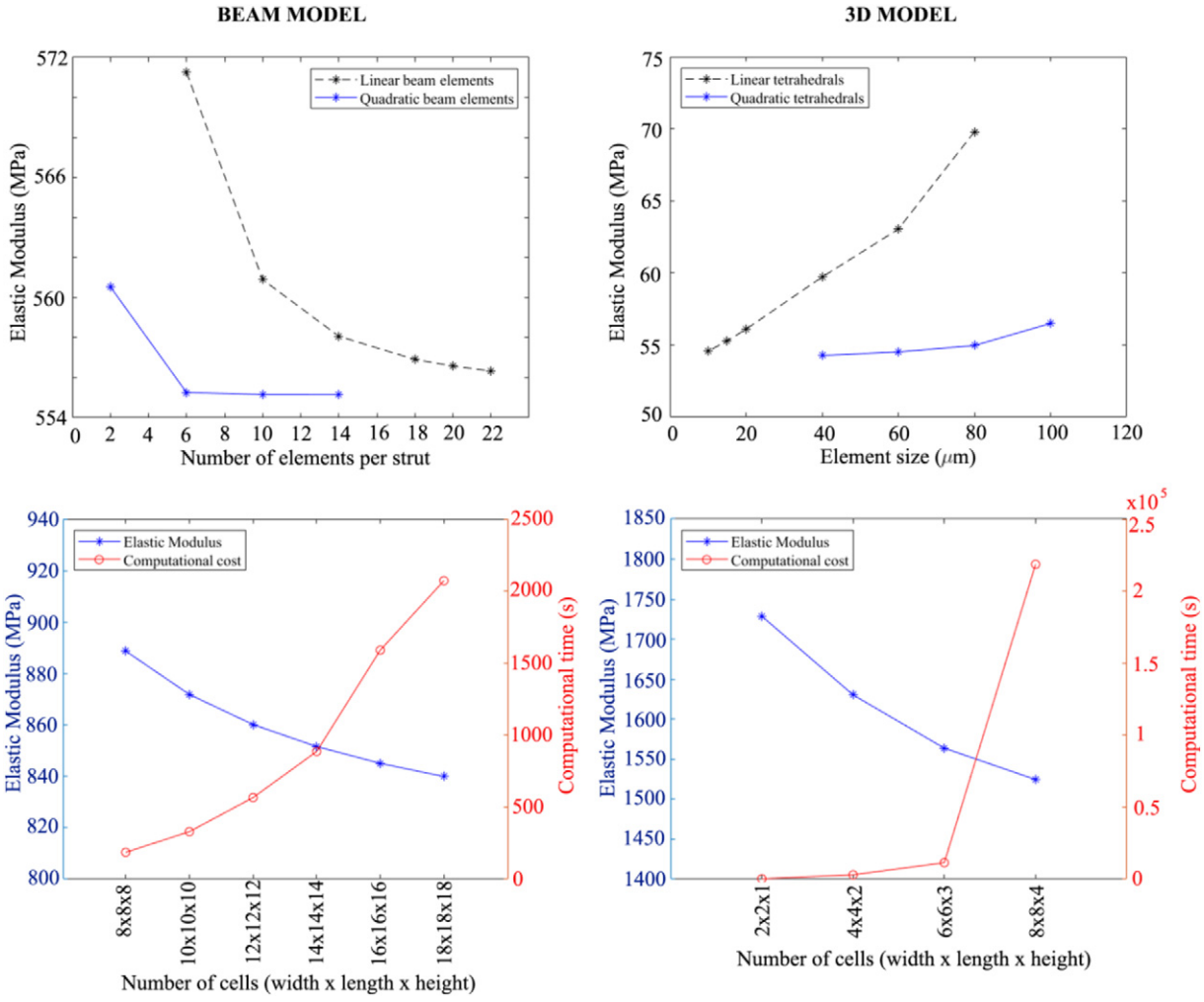

Fig. 5. Element size and number of cells sensitivity analysis for the beam model (left) and the solid mesh (right) for the FCC structure.

unit cells in the height is enough to reach convergence, however, when applying a friction coefficient of 0.3, 10–11 unit cells are required to reach convergence. For a bonded contact, the structure was modelled up to 13 unit cells in the height, but convergence was not achieved. Fig. 8 (right) illustrates the difference in the elastic modulus based on the different boundary conditions. When a frictionless contact is applied, the elastic modulus of the structure is 267.34 MPa, and as the friction coefficient is increased to 0.3, the elastic modulus rises to 327.35 MPa, an increase of 22.5%. This difference would be even greater for the bonded contact.

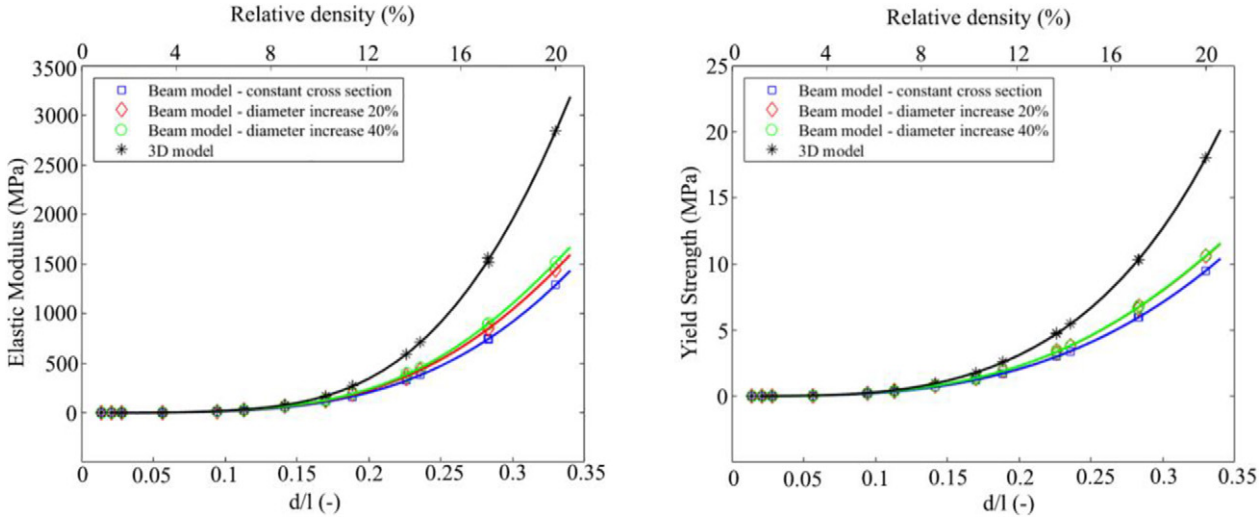

Fig. 6. Elastic modulus and yield strength for FCC lattices with different relative densities for the beam and 3D models.

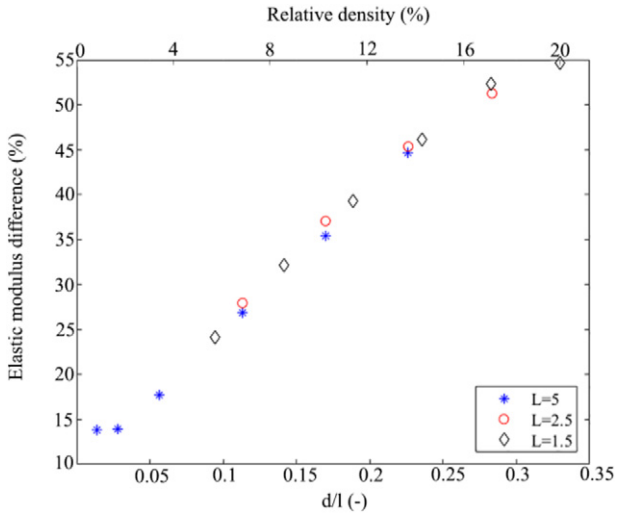

Fig. 7. Elastic modulus difference between the 3D mesh and beam model with constant cross section (L denotes the unit cell size) for the FCC structure.

3.3. Material model

The average diameter, elastic modulus, yield strength and ultimate strength values for each of the single struts are shown in Table 2.

As expected, due to irregularities in the manufacturing process such as internal porosity, diameter variation or semi-fused powder (Fig. 9), as well as due to the test conditions, variations in mechanical properties were observed for each strut diameter (Table 2). The modulus of the struts varied between 68.9 and 98.8 GPa. These values are around 60% lower than the bulk material and within the range found in other studies [6,16].

As mentioned earlier, an average stress-strain curve was produced and consequently two bilinear elasto-plastic models were derived and shown in Table 3. These two models together with the stress-strain curve are illustrated in Fig. 10.

The effect of the material model on the FCC FEA results are seen in Fig. 11 (left). Results are very similar when defining the material either with the average stress-strain-curve of the struts or with elasto-plastic model B, where the structure's yield strength differs by 3.8%. However, when elasto-plastic model A is used, this difference increases to 15.6%. Strut 1 and 4, which have the greatest yield strength and stiffness deviation with respect to the average model, were also used to generate elasto-plastic models as per elasto-plastic model B generated from the average strut stress-strain curve. The difference in stiffness and yield strength between the material model of strut 1 and average material model is 5.8% and 5.2% respectively. This difference results in a variation of the lattice structure stiffness of 8.4% and yield strength of 4.9%. When using the material model of strut 4, which has a stiffness and yield strength difference of 13.2% and 1.8% with respect to the average material model, the lattice structure stiffness and yield strength consequently differ by 10.5% and 4.4%.

3.4. Compression test results

It was found that for a given laser parameter, strut thickness in the porous structure was slightly larger than when manufacturing single struts. The measured values are shown in Table 4. This is likely due to residual heat being present when manufacturing a porous structure where struts are in close proximity to each other rather than single struts placed far apart. When observing the manufactured lattice structures under SEM (Fig. 12), there is a clear difference in surface morphology between the upward facing surfaces (upskin) of the struts versus the downward facing surfaces (downskin). There also appears to be some mild thinning of some struts near intersections/nodes as well as distortion of nodes and strut 'waviness' is more apparent on thin long struts.

Regardless of unit cell size or strut thickness all porous structures displayed a ductile failure and similar failure modes/failure planes (Fig. 13).

The experimental results of the elastic modulus and yield strength for both structures are represented in Table 5 and illustrated in Fig. 14 for the FCC structure. Regardless of structure and unit cell size, both apparent modulus and yield strength vary by a power-law with respect to relative density as per Gibson and Ashby [29,32].

3.5. FEA vs experiments

Fig. 14 and Table 6 illustrates the elastic modulus and yield strength of both the experimental compression tests and the FEA results. For the FCC, the average error between the experimental and FEA results for the elastic modulus and yield strength was 10.99% (6.91%) and 17.77% (15.26%), respectively. The maximum difference between the FEA and

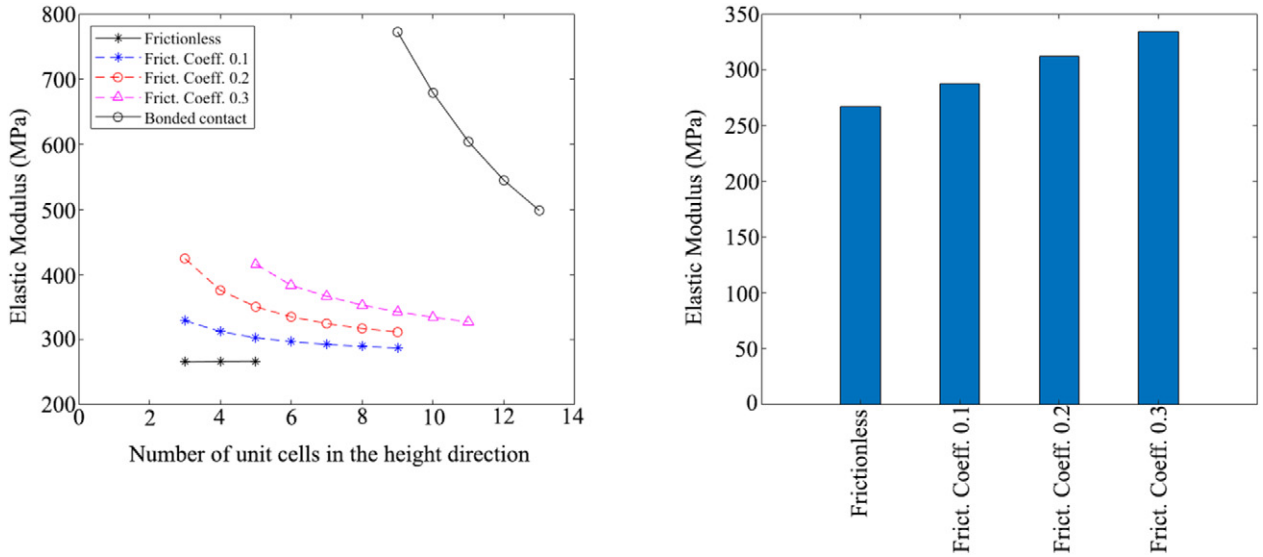

Fig. 8. Elastic modulus and yield strength based on the contact properties for the FCC Structure.

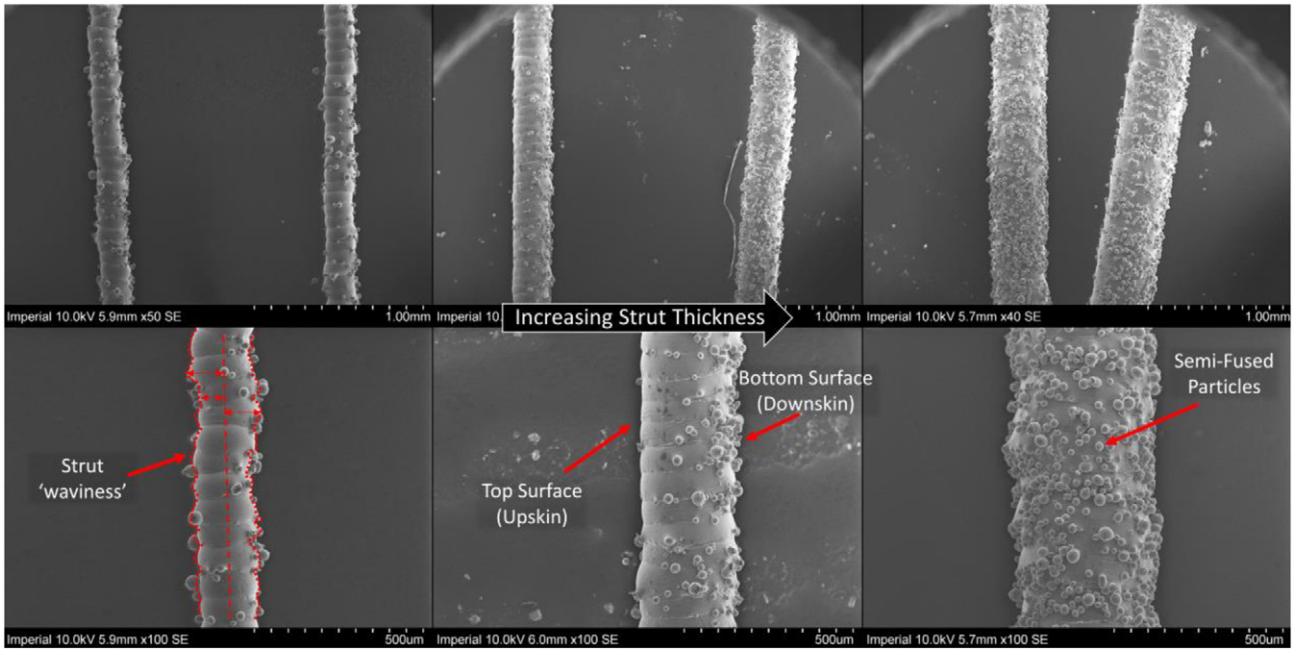

Fig. 9. SEM images of different struts. From left to right struts of increasing diameter. Top row: ×50 magnification. Bottom row: x100 magnification.

the experiments for the elastic modulus and yield strength are 21.5% (FCC 8) and 42.2% (FCC 5), respectively. The FEA was also able to mimic the failure mechanics and yielding behaviour of the modified FCC structure (Fig. 13c).

To further determine the accuracy of the FE approach, the OCT structure was numerically simulated as well as manufactured and tested experimentally. The average error between the FEA and experiments for the OCT structure was 8.50% (6.67%) and 17.02% (2.44%) for the elastic modulus and yield strength, respectively.

4. Discussion

This work has explored the various methodologies and variables necessary to build FEA models of lattice structures and has compared them to experimental compression testing for two different structures. The study highlights how modelling the appropriate number of unit cells, altering the boundary conditions or material model can drastically affect the outputs of the simulation. A systematic study of these variables is necessary to have confidence in the results and reliability of the simulation. The methodology presented in this work (Fig. 15) should provide a foundation to build future models for other lattice structures comprising non-stochastic or periodic unit cells as well as more complex structures such as functionally graded materials.

When working with lattice structures with large d/l ratios, a solid mesh is suggested. In this study it was found that for d/l ratios >0.1, the mechanical properties can differ by >20% between the solid 3D mesh and beam models. This difference seems to increase linearly with the d/l ratio. Whilst, these findings were obtained for the modified FCC unit cell, it should be seen whether the same is true for other unit cells. Although many lattice FEA studies consider a frictionless contact between the platens and samples [5,6,13,14], a barrelling effect was observed experimentally in the tested samples, indicating that friction was present. Whilst, other studies account for this friction in their models with friction coefficients equal to 0.2 [33,34], 0.9 [17] or even bonded contacts [11,18]. In this work it was observed that the difference in modulus between considering a frictionless contact and a friction coefficient of 0.2 is 16.5%, and 22.5% if considering a friction coefficient of 0.3. Altering the applied boundary condition will also change how many unit cells are necessary in the height to ensure convergence of the mechanical properties. In this work, the convergence for the bonded contact boundary condition was not achieved (a height of 13 unit cells was studied), but the trend indicates that the difference in the elastic modulus between a frictionless contact and a bonded contact is ~50%.

It was found that defining the material model in FEA simulations with the bilinear elasto-plastic model B derived from the strut tensile tests was accurate. The procedure highlights that using the bulk material properties would not be accurate unless the actual strut geometry,

Table 3
Young's modulus, yield stress, ultimate strength and ultimate plastic strain of the elasto-plastic models.

Elasto-plastic model	Young's modulus [GPa]	Yield stress [MPa]	Ultimate strength [MPa]	Ultimate plastic strain [−]
A	81.3	300.2	575.3	0.19
B	81.3	263.3	575.3	0.22

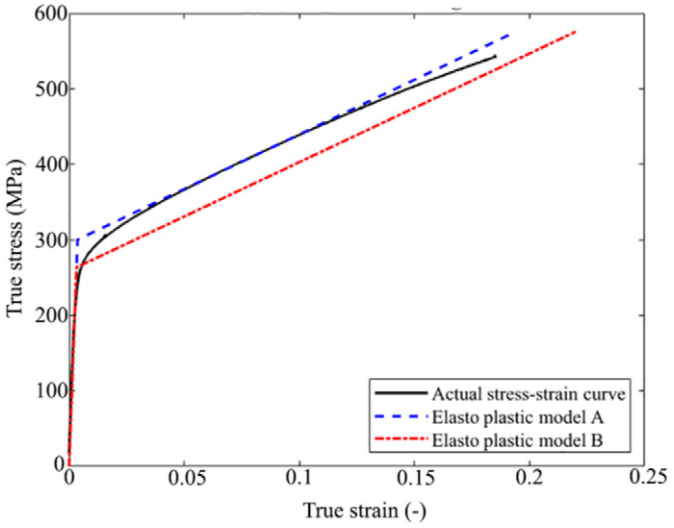

Fig. 10. Experimentally derived average stress-strain curve for single struts. Elasto-plastic material models constructed from experimental results using two different methods of extracting yield stress and subsequent strain.

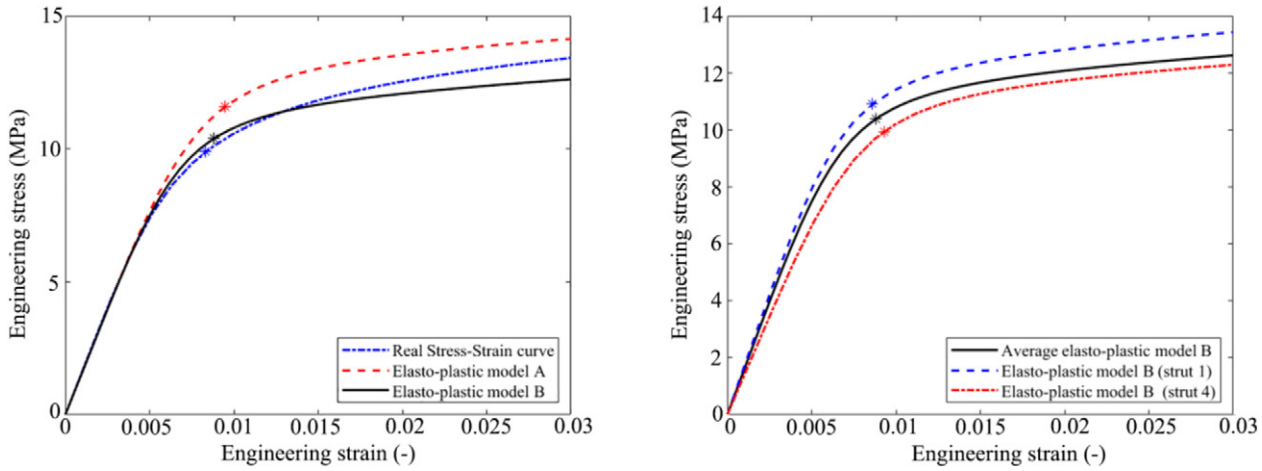

Fig. 11. Stress-strain curves for the FCC structure comparing the elasto-plastic models with the actual stress-strain curve (left); and elasto-plastic model B derived from the average strut, strut 1 and strut 4, which deviate the most from the average strut stress-strain curve (right).

imperfections and deviations were modelled. Using the mechanical properties from tensile testing of an individual strut and modelling the struts at a constant diameter is simpler and consequently includes the imperfections in the model. Over the range of diameters tested in this study for stainless steel, the mechanical properties of the struts did not differ greatly with increasing strut diameter. When comparing FEA results using the average strut material model versus the mechanical properties from the strut with the greatest difference in properties (Strut 4), only resulted in differences in lattice structure modulus of 13.2%. Therefore, for stainless steel and for the range of strut diameters tested in this study, using an average material model rather that a structure/strut specific model can be considered as a good approximation.

For both the FEA simulations and the experimental testing the relationship between modulus, yield strength and relative density followed models described by Gibson and Ashby [29,32] seen in Eqs. (1) and (2). Stress/Strength (σ) and modulus (E) increase with density (ρ) by a power law. This relationship was found to be true for AM structures by a number of authors [2,13,23,24,30,31] and can be seen in Fig. 14.

$$\frac{\sigma}{\sigma_0} = C_1\left(\frac{\rho}{\rho_0}\right)^n \tag{1}$$

$$\frac{E}{E_0} = C_2\left(\frac{\rho}{\rho_0}\right)^m \tag{2}$$

where σ_0, ρ_0 and E_0 are the properties of the base material (i.e. solid stainless steel) and C, m and n are constants found experimentally. It is important to note these equations are only accurate to a relative density of 0.3 [29].When comparing the experimental results to the final FEA simulations differences in the moduli were on average (s.d.) 10.99% (6.91%) and 8.50% (6.67%) for the FCC and OCT structures respectively. There are however, a number of sources of error still likely present. As mentioned earlier, a barrelling effect was observed in the tested structures and therefore a friction coefficient of 0.1 was applied in the FEA. This value is likely close to reality when applying lubrication to the platens but needs further validation. Small errors when measuring the strut diameter would affect the 3D structure designed in PTC CREO. These errors would have more impact on the 1.5 unit cells as the variation in the relative density would be greater than in the 2.5 unit cells. Larger differences of on average ~17% for each structure were seen in yield strength when comparing the experimental results to the FEA. Apart from the afore-mentioned sources of errors, it was observed that also using the elasto-plastic material model instead of the actual stress-strain curve of the material results in an increase of the yield strength in the FEA of around 4%. Yield strength can be over-predicted in FEA due to the idealised cylindrical shape of the struts. It is also clear from the SEM images that a number of structural irregularities are present such as strut waviness, non-idealised strut intersections/nodes, differences in surface morphology between upward and downward faces surfaces and crack initiation sites. There is also a limitation on measuring strut thickness from SEM images and not μCT scans as it assumes the cross-section is a perfect circle. At a 45° build angle and as multiple individual struts were measured with a low standard deviation it can be assumed the struts were quite cylindrical but it is possible with different diameters and build angles this may not always be the case. To combat this, μCT scanning of individual struts and lattice structures can better inform the shape and size of the struts. Finally, there is likely residual stress and a level of self-stress in the structure that is not accounted for in the FEA, possibly stress-relieving the specimens could reduce the errors found.

The mismatch found in this work between the predicted FEA results and the experiments are acceptable and generally lower than found in literature. Table 7 displays the elastic modulus differences obtained in other works following various FE methodologies.

Table 4
Strut diameters measured from the single struts and the lattice structures.

Strut (laser parameters: power – exposure time – point distance)	Single strut [μm] (s.d.)	FCC 1.5 mm unit Cell [μm] (s.d.)	FCC 2.5 mm unit cell [μm] (s.d.)	OCT 1.5 mm unit cell [μm] (s.d.)
1 (125 W-70 μs-50 μm)	176.9 (9.0)	210.5 (8.3)	201.6 (7.4)	201.8 (10.5)
2 (125 W-100 μs-50 μm)	205.8 (10.1)	229.3 (9.1)	–	–
3 (125 W-200 μs-50 μm)	247.8 (13.9)	277.1 (10.6)	282.2 (6.9)	289.1 (14.0)
4 (125 W-300 μs-50 μm)	289.2 (15.5)	336.6 (14.9)	–	–
5 (125 W-450 μs-50 μm)	325.5 (12.9)	359.8 (13.2)	365.5 (15.6)	365.1 (11.6)
6 (125 W-600 μs-50 μm)	362.1 (11.9)	–	411.4 (12.8)	–
7 (125 W-800 μs-50 μm)	408.7 (18.8)	–	443.6 (15.3)	–

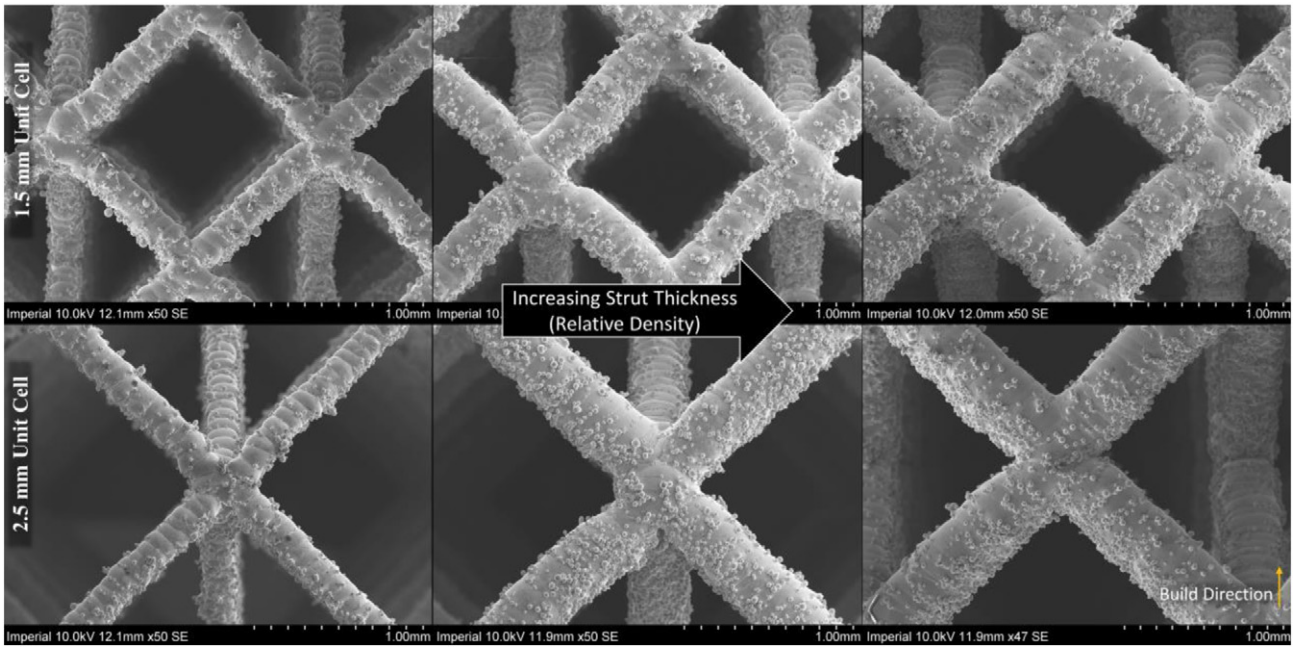

Fig. 12. SEM images of FCC Lattices.

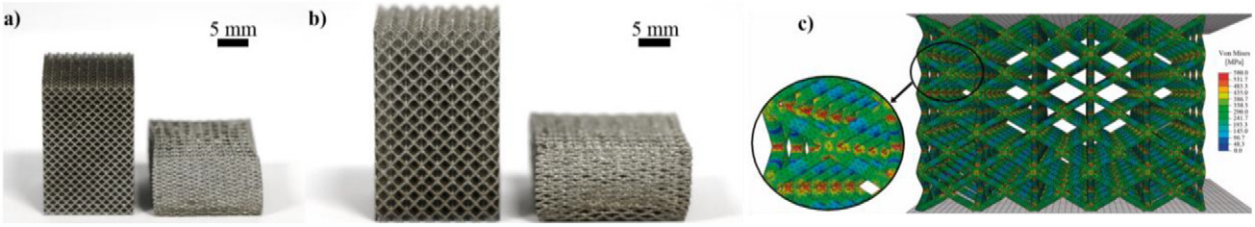

Fig. 13. a) 1.5 mm unit cell and b) 2.5 mm unit cell FCC structures in as-built and compressed to ~50% strain conditions. c) FEA simulated stress distribution in a FCC at 25% strain.

The first four works displayed in Table 7 considered strut irregularities when modelling the lattice structure. In the recent work carried out by Lei et al. [33] all the structures were scanned by μCT to implement the actual irregularities in the FEA model, however the struts were modelled with beam elements and the structure had a small d/l ratio. In our work, it was found that modelling the lattice structure with beam elements instead of tetrahedral elements underestimates the apparent elastic modulus of the lattice structure for large d/l ratios and thus it is possible their methodology would produce larger errors for structures with greater d/l ratios. The error obtained by Kadkhodapour et al. [12] was 10% for a diamond unit cell and 63% for a cubic unit cell. Although strut irregularities are known to happen during the manufacturing process, in their work irregularities were not added to the model nor in the geometry nor in the material model. In the work by Smith et al. [5] the difference found in the elastic modulus was only 15%, in the range of this study. In Smith et al.'s work the material properties of stainless-steel were used and a reverse engineering method was used to find the effective diameter of the struts. In this reverse engineering method, the strut diameter was

Table 5
Experimental elastic modulus and yield strength of specimens.

Structure	Strut # (Table 4)	Unit cell size [mm]	FEA # elements	Strut diameter [μm] (s.d.)	Elastic modulus [MPa] (s.d.)	Yield strength [MPa] (s.d.)
FCC1	1	2.5	496,834	201.6 (7.4)	36.0 (0.8)	0.41 (0.00)
FCC2	3	2.5	546,907	282.2 (6.9)	177.4 (3.8)	1.45 (0.03)
FCC3	5	2.5	458,514	365.5 (15.6)	531.0 (7.1)	3.42 (0.03)
FCC4	6	2.5	471,564	411.4 (12.8)	713.0 (47.0)	4.25 (0.19)
FCC5	7	2.5	589,413	443.6 (15.3)	920.5 (61.9)	5.26 (0.19)
FCC6	1	1.5	732,343	210.5 (8.3)	343.8 (15.7)	2.52 (0.07)
FCC7	2	1.5	749,729	229.3 (9.1)	674.2 (35.9)	4.36 (0.14)
FCC8	3	1.5	917,424	277.1 (10.6)	1580.8 (64.0)	8.76 (0.26)
FCC9	4	1.5	504,449	336.6 (14.9)	3038.2 (60.6)	16.12 (0.11)
FCC10	5	1.5	552,426	359.8 (13.2)	3569.7 (193.4)	19.92 (0.11)
OCT1	1	1.5	1,368,089	201.8 (10.5)	751.1 (5.4)	5.24 (0.02)
OCT2	3	1.5	1,216,099	289.1 (14.0)	3265.1 (138.2)	18.87 (0.36)
OCT3	5	1.5	1,066,861	365.1 (11.6)	7319.7 (136.3)	39.94 (0.14)

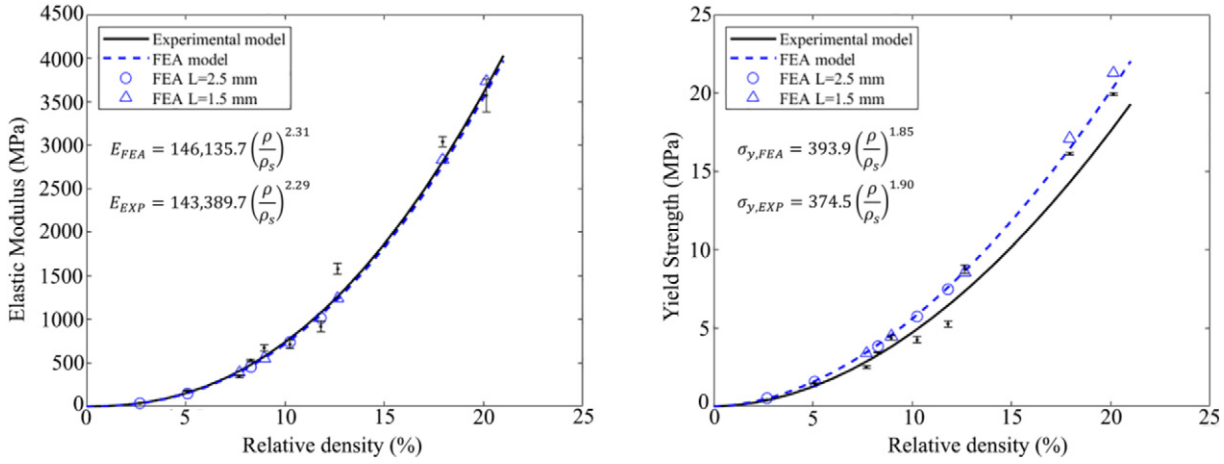

Fig. 14. Experiments vs FEA results for the FCC structure. Elastic modulus (left) and yield strength (right).

varied until both the experiment and FE stress-strain curves coincided. This approach is performed for every model and strut diameter and has the drawback of experimental data being required. The procedure described in this study, which gives accurate results, better represents reality by utilising the actual diameter and material properties measured from the struts.

In this work two bending-dominated structures were studied and although one can expect similar results with other unit cell types, this should be studied in more detail before extrapolating the results. For instance, the results for stretch-dominated, stochastic or graded structures may differ due to the different deformation mechanisms. However, a similar procedure to the one described in this work can likely be followed to study these structures. In contrast, for triply periodic and surface based porous structures, more work should be performed in the future to define an accurate FEA procedure, particularly in defining the material model (as this study derived the material model from tensile testing of struts) and the minimum area to model. Future work should also look at studying the behaviour of the studied structures in other directions and under different load conditions such as shear or bending.

5. Conclusion

In this study a procedure to build and validate a finite-element model for additively manufactured metal lattice structures has been described. The results of the simulation were compared to experimental compression testing for a modified FCC and OCT lattice and showed good agreement (the average errors for the modulus and yield strength were 9–11% and 18% respectively) over a range of strut diameters (relative densities) and unit cell sizes whilst trying to minimize computational cost. It was also found that structure geometry can inform what modelling approach to use. When working with lattice structures with large d/l ratios, a solid mesh is suggested. For d/l ratios >0.1, the mechanical properties can differ by >20% between the solid 3D mesh and beam models. This difference seems to increase linearly with the d/l ratio. However, for small d/l ratios the beam model approximation can be appropriate. This study has also shown how boundary conditions can affect the minimum size of the structure that has to be modelled in order to achieve convergence. Finally, the study highlights how finite-element models of lattice structures are heavily dependent on the material model and boundary conditions and that accurate representation of the actual material and test conditions are necessary to obtain reliable results that can be used with confidence.

Credit authorship contribution statement

Sergio Ruiz de Galarreta: Conceptualization, Methodology, Formal analysis, Investigation, Writing - original draft. **Jonathan R.T. Jeffers:** Writing - review & editing, Supervision, Funding acquisition. **Shaaz Ghouse:** Conceptualization, Validation, Investigation, Writing - review & editing.

Table 6
Experimental vs FEA results for the FCC and OCT structures.

Structure	Modulus			Yield strength		
	FEA [MPa]	Experimental [MPa]	Difference	FEA [MPa]	Experimental [MPa]	Difference
FCC1	35.8	36.0	0.5%	0.52	0.41	26.8%
FCC2	148.2	177.4	16.4%	1.59	1.45	9.4%
FCC3	453.6	531.0	14.6%	3.84	3.42	12.3%
FCC4	740.1	713.0	3.8%	5.74	4.25	35.1%
FCC5	1014.9	920.5	10.3%	7.48	5.26	42.2%
FCC6	388.7	343.8	13.0%	3.39	2.52	34.5%
FCC7	550.6	674.2	18.3%	4.46	4.36	2.3%
FCC8	1241.4	1580.8	21.5%	8.55	8.76	2.4%
FCC9	2828.6	3038.2	6.9%	17.08	16.12	6.0%
FCC10	3734.5	3569.7	4.6%	21.26	19.92	6.7%
OCT1	704.3	751.1	6.2%	6.2	5.24	17.8%
OCT2	3321.0	3265.1	1.7%	21.5	18.87	13.7%
OCT3	8606.3	7319.7	17.6%	47.8	39.94	19.6%

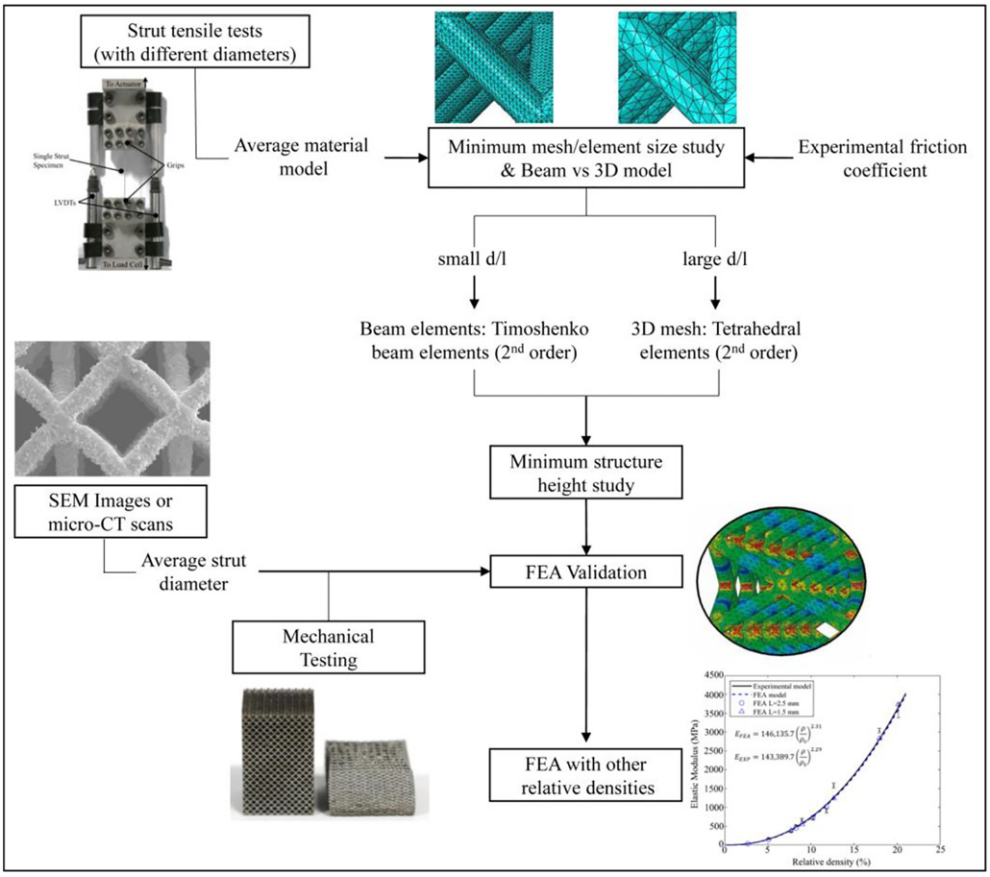

Fig. 15. Diagram of the proposed FEA procedure.

Declaration of competing interest

The authors declare that they have no known competing financial interests or personal relationships that could have appeared to influence the work reported in this paper.

Acknowledgements

The authors wish to gratefully acknowledge the Engineering and Physical Sciences Research Council (EP/R042721/1) and the Wellcome Trust (208858/Z/17/Z) for their financial support of this study.

Data availability

The raw data required to reproduce these findings are available to download from rdm-enquiries@imperial.ac.uk. The processed data required to reproduce these findings are available to download from rdm-enquiries@imperial.ac.uk.

Table 7
Elastic modulus difference between FEA and experiments in the literature.

Authors	Unit cell	Difference FEA and experiments (%)
Hazlehurst et al. [35]	Cubic	333
Karamooz Ravari et al. [36]	BCC	91
Gonzalez et al. [18]	Cubic	92
Lei et al. [33]	BCC	45
	BCC-Z	5
Lozanovski et al. [17]	FCC	23
	FCZ	56
Kadkhodapour et al. [12]	Diamond	10
	Cubic	63
Smith et al. [5]	BCC	15

References

[1] M. Rashed, M. Ashraf, R. Mines, P.J. Hazell, Metallic microlattice materials: a current state of the art on manufacturing, mechanical properties and applications, Mater. Des. 95 (2016) 518–533. https://doi.org/10.1016/j.matdes.2016.01.146.
[2] V.J. Challis, X. Xu, L.C. Zhang, A.P. Roberts, J.F. Grotowski, T.B. Sercombe, High specific strength and stiffness structures produced using selective laser melting, Mater. Des. 63 (2014) 783–788, https://doi.org/10.1016/j.matdes.2014.05.064.
[3] M.E. Lynch, M. Mordasky, L. Cheng, A. To, Design, testing, and mechanical behavior of additively manufactured casing with optimized lattice structure, Addit. Manuf. 22 (2018) 462–471, https://doi.org/10.1016/j.addma.2018.05.021.
[4] S. Ghouse, N. Reznikov, O.R. Boughton, S. Babu, K.C.G. Ng, G. Blunn, J.P. Cobb, M.M. Stevens, J.R.T. Jeffers, The design and in vivo testing of a locally stiffness-matched porous scaffold, Appl. Mater. Today 15 (2019) 377–388, https://doi.org/10.1016/j.apmt.2019.02.017.
[5] M. Smith, Z. Guan, W.J. Cantwell, Finite element modelling of the compressive response of lattice structures manufactured using the selective laser melting technique, Int. J. Mech. Sci. 67 (2013) 28–41, https://doi.org/10.1016/j.ijmecsci.2012.12.004.
[6] R. Gümrük, R.A.W. Mines, Compressive behaviour of stainless steel micro-lattice structures, Int. J. Mech. Sci. 68 (2013) 125–139, https://doi.org/10.1016/j.ijmecsci.2013.01.006.
[7] S.M. Ahmadi, G. Campoli, S. Amin Yavari, B. Sajadi, R. Wauthle, J. Schrooten, H. Weinans, A.A. Zadpoor, Mechanical behavior of regular open-cell porous biomaterials made of diamond lattice unit cells, J. Mech. Behav. Biomed. Mater. 34 (2014) 106–115, https://doi.org/10.1016/j.jmbbm.2014.02.003.
[8] M. Alaña, A. López de Arancibia, A. Pradera-Mallabiabarrena, S. Ruiz de Galarreta, Analytical model of the elastic behavior of a modified face-centered cubic lattice structure, J. Mech. Behav. Biomed. Mater. 98 (2019) 357–368, https://doi.org/10.1016/j.jmbbm.2019.05.043.
[9] M. Zhang, Z. Yang, Z. Lu, B. Liao, X. He, Effective elastic properties and initial yield surfaces of two 3D lattice structures, Int. J. Mech. Sci. 138–139 (2018) 146–158, https://doi.org/10.1016/j.ijmecsci.2018.02.008.
[10] F.J. Quevedo González, N. Nuño, Finite element modelling approaches for well-ordered porous metallic materials for orthopaedic applications: cost effectiveness and geometrical considerations, Comput. Methods Biomech. Biomed. Engin. 19 (2016) 845–854, https://doi.org/10.1080/10255842.2015.1075009.
[11] M.R. Karamooz Ravari, M. Kadkhodaei, M. Badrossamay, R. Rezaei, Numerical investigation on mechanical properties of cellular lattice structures fabricated by fused deposition modeling, Int. J. Mech. Sci. 88 (2014) 154–161, https://doi.org/10.1016/j.ijmecsci.2014.08.009.

[12] J. Kadkhodapour, H. Montazerian, A.C. Darabi, A.P. Anaraki, S.M. Ahmadi, A.A. Zadpoor, S. Schmauder, Failure mechanisms of additively manufactured porous biomaterials: effects of porosity and type of unit cell, J. Mech. Behav. Biomed. Mater. 50 (2015) 180–191, https://doi.org/10.1016/j.jmbbm.2015.06.012.
[13] V. Crupi, E. Kara, G. Epasto, E. Guglielmino, H. Aykul, Static behavior of lattice structures produced via direct metal laser sintering technology, Mater. Des. 135 (2017) 246–256, https://doi.org/10.1016/j.matdes.2017.09.003.
[14] D. Melancon, Z.S. Bagheri, R.B. Johnston, L. Liu, M. Tanzer, D. Pasini, Mechanical characterization of structurally porous biomaterials built via additive manufacturing: experiments, predictive models, and design maps for load-bearing bone replacement implants, Acta Biomater. 63 (2017) 350–368, https://doi.org/10.1016/j.actbio.2017.09.013.
[15] J. Kadkhodapour, H. Montazerian, A.C. Darabi, A. Zargarian, S. Schmauder, The relationships between deformation mechanisms and mechanical properties of additively manufactured porous biomaterials, J. Mech. Behav. Biomed. Mater. 70 (2017) 28–42, https://doi.org/10.1016/j.jmbbm.2016.09.018.
[16] P. Li, Z. Wang, N. Petrinic, C.R. Siviour, Deformation behaviour of stainless steel microlattice structures by selective laser melting, Mater. Sci. Eng. A 614 (2014) 116–121, https://doi.org/10.1016/j.msea.2014.07.015.
[17] B. Lozanovski, M. Leary, P. Tran, D. Shidid, M. Qian, P. Choong, M. Brandt, Computational modelling of strut defects in SLM manufactured lattice structures, Mater. Des. 171 (2019), 107671. https://doi.org/10.1016/j.matdes.2019.107671.
[18] F.J.Q. Gonzalez, N. Nuno, Finite element modeling of manufacturing irregularities of porous materials, Biomater. Biomech. Bioeng. 3 (2016) 1–14. https://doi.org/10.12989/bme.2016.3.1.001.
[19] J. Souza, A. Großmann, C. Mittelstedt, Micromechanical analysis of the effective properties of lattice structures in additive manufacturing, Addit. Manuf. 23 (2018) 53–69, https://doi.org/10.1016/j.addma.2018.07.007.
[20] G.N. Labeas, M.M. Sunaric, Investigation on the static response and failure process of metallic open lattice cellular structures, Strain 46 (2010) 195–204, https://doi.org/10.1111/j.1475-1305.2008.00498.x.
[21] M.H. Luxner, J. Stampfl, H.E. Pettermann, Finite element modeling concepts and linear analyses of 3D regular open cell structures, J. Mater. Sci. 40 (2005) 5859–5866, https://doi.org/10.1007/s10853-005-5020-y.
[22] C. Neff, N. Hopkinson, N.B. Crane, Experimental and analytical investigation of mechanical behavior of laser-sintered diamond-lattice structures, Addit. Manuf. 22 (2018) 807–816, https://doi.org/10.1016/j.addma.2018.07.005.
[23] Y. Xu, D. Zhang, S. Hu, R. Chen, Y. Gu, X. Kong, J. Tao, Y. Jiang, Mechanical properties tailoring of topology optimized and selective laser melting fabricated Ti6Al4V lattice structure, J. Mech. Behav. Biomed. Mater. 99 (2019) 225–239, https://doi.org/10.1016/j.jmbbm.2019.06.021.
[24] H. Mehboob, F. Tarlochan, A. Mehboob, S.H. Chang, Finite element modelling and characterization of 3D cellular microstructures for the design of a cementless biomimetic porous hip stem, Mater. Des. 149 (2018) 101–112, https://doi.org/10.1016/j.matdes.2018.04.002.
[25] J. Wieding, A. Wolf, R. Bader, Numerical optimization of open-porous bone scaffold structures to match the elastic properties of human cortical bone, J. Mech. Behav. Biomed. Mater. 37 (2014) 56–68, https://doi.org/10.1016/j.jmbbm.2014.05.002.
[26] G. Campoli, M.S. Borleffs, S. Amin Yavari, R. Wauthle, H. Weinans, A.A. Zadpoor, Mechanical properties of open-cell metallic biomaterials manufactured using additive manufacturing, Mater. Des. 49 (2013) 957–965, https://doi.org/10.1016/j.matdes.2013.01.071.
[27] S. Tsopanos, R. Mines, S. McKown, Y. Shen, J. Cantwell, W. Brooks, C. Sutcliffe, The influence of processing parameters on the mechanical properties of selectively laser melted stainless steel microlattice structures, J. Manuf. Sci. Eng. 132 (2010).
[28] M. Ashby, T. Evans, N. Fleck, J. Hutchinson, H. Wadley, L. Gibson, Metal Foams A Design Guide, Elsevier, 2000.
[29] L.J. Gibson, M.F. Ashby, Cellular Solids, Cambridge University Press, Cambridge, 1997https://doi.org/10.1017/CBO9781139878326.
[30] S. Ghouse, S. Babu, K. Nai, P.A. Hooper, J.R.T. Jeffers, The influence of laser parameters, scanning strategies and material on the fatigue strength of a stochastic porous structure, Addit. Manuf. 22 (2018) 290–301, https://doi.org/10.1016/j.addma.2018.05.024.
[31] S. Ghouse, S. Babu, R.J. Van Arkel, K. Nai, P.A. Hooper, J.R.T. Jeffers, The influence of laser parameters and scanning strategies on the mechanical properties of a stochastic porous material, Mater. Des. 131 (2017) 498–508, https://doi.org/10.1016/j.matdes.2017.06.041.
[32] M.F. Ashby, The properties of foams and lattices, Philos. Trans. R. Soc. A Math. Phys. Eng. Sci. 364 (2006) 15–30, https://doi.org/10.1098/rsta.2005.1678.
[33] H. Lei, C. Li, J. Meng, H. Zhou, Y. Liu, X. Zhang, P. Wang, D. Fang, Evaluation of compressive properties of SLM-fabricated multi-layer lattice structures by experimental test and μ-CT-based finite element analysis, Mater. Des. 169 (2019), 107685. https://doi.org/10.1016/j.matdes.2019.107685.
[34] M. Mahbod, M. Asgari, Elastic and plastic characterization of a new developed additively manufactured functionally graded porous lattice structure: analytical and numerical models, Int. J. Mech. Sci. 155 (2019) 248–266, https://doi.org/10.1016/j.ijmecsci.2019.02.041.
[35] K. Hazlehurst, C.J. Wang, M. Stanford, Evaluation of the stiffness characteristics of square pore CoCrMo cellular structures manufactured using laser melting technology for potential orthopaedic applications, Mater. Des. 51 (2013) 949–955, https://doi.org/10.1016/j.matdes.2013.05.009.
[36] M.R. Karamooz Ravari, M. Kadkhodaei, A computationally efficient modeling approach for predicting mechanical behavior of cellular lattice structures, J. Mater. Eng. Perform. 24 (2015) 245–252, https://doi.org/10.1007/s11665-014-1281-4.